

# MIMO Systems Aided by Microwave Linear Analog Computers: Capacity-Achieving Architectures with Reduced Circuit Complexity

Matteo Nerini, *Member, IEEE*, and Bruno Clerckx, *Fellow, IEEE*

**Abstract**—To meet the demands of future wireless networks, antenna arrays must scale from massive multiple-input multiple-output (MIMO) to gigantic MIMO, involving even larger numbers of antennas. To address the hardware and computational cost of gigantic MIMO, several strategies are available that shift processing from the digital to the analog domain. Among them, microwave linear analog computers (MiLACs) offer a compelling solution by enabling fully analog beamforming through reconfigurable microwave networks. Prior work has focused on fully-connected MiLACs, whose ports are all interconnected to each other via tunable impedance components. Although such MiLACs are capacity-achieving, their circuit complexity, given by the number of required impedance components, scales quadratically with the number of antennas, limiting their practicality. To solve this issue, in this paper, we propose a graph theoretical model of MiLAC facilitating the systematic design of lower-complexity MiLAC architectures. Leveraging this model, we propose stem-connected MiLACs as a family of MiLAC architectures maintaining capacity-achieving performance while drastically reducing the circuit complexity. Besides, we optimize stem-connected MiLACs with a closed-form capacity-achieving solution. Our theoretical analysis, confirmed by numerical simulations, shows that stem-connected MiLACs are capacity-achieving, but with circuit complexity that scales linearly with the number of antennas, enabling high-performance, scalable, gigantic MIMO.

**Index Terms**—Capacity, gigantic MIMO, graph theory, microwave linear analog computer (MiLAC)

## I. INTRODUCTION

As wireless systems evolve toward sixth-generation (6G), the demand for ultra-high data rates, low latency, and pervasive connectivity continues to increase, pushing beyond the capabilities of fifth-generation (5G) technologies. While massive multiple-input multiple-output (MIMO) systems, typically including tens of antennas, have proven successful in 5G [1], [2], 6G requires a further substantial increase in the number of antennas. This emerging paradigm, denoted as gigantic MIMO, envisions MIMO architectures with antenna arrays scaling to the order of thousands of antennas [3], [4]. Such extreme scaling offers significant enhancements in spatial multiplexing and beamforming resolution, which are critical to meet 6G targets in the anticipated upper mid-band spectrum (7-24 GHz). However, traditional digital MIMO architectures are not suited to this scale due to the prohibitive cost, power consumption,

and complexity of assigning one radio frequency (RF) chain per antenna, each requiring high-resolution analog-to-digital converters (ADCs)/digital-to-analog converters (DACs) and mixers. This challenge has steered research efforts toward analog-domain solutions, which can provide more scalable, cost-effective, and energy-efficient alternatives to fully digital MIMO architectures.

Hybrid digital-analog MIMO architectures originally emerged to reduce the demand of RF chains while preserving high performance through the use of analog phase shifters [5], [6]. Another technology classically used to change the radiation pattern of an antenna array operating in the analog domain is reconfigurable antennas [7]. The idea of reconfigurable antennas traces back to the 1930s, when they were realized through mechanically moving parts. Since the 1990s, reconfigurable antennas have been realized by interconnecting parts of the antenna through tunable components, such as varactors, mechanical RF switches, or semiconductor RF switches. To synergize the benefits of hybrid beamforming and the recent advances in reconfigurable antennas, the tri-hybrid MIMO architecture has been recently proposed [8], where the signal is processed in three stages: digitally, in the analog domain by phase shifts, and in the electromagnetic (EM) domain by reconfigurable antennas.

Beamforming in the analog domain can also be achieved through the use of intelligent reflecting surfaces (IRSs), also known as reconfigurable intelligent surfaces (RISs). A RIS is a surface made of a multitude of elements with reconfigurable scattering capabilities, which can be integrated at the transceiver device to reconfigure its effective radiation pattern [9], [10]. To enhance the flexibility of RIS, the concept of beyond diagonal RIS (BD-RIS) has emerged, where the RIS elements are interconnected to each other through tunable interconnections [11], [12], [13]. Furthermore, the use of multiple stacked RISs has been explored to increase adaptability, giving rise to stacked intelligent metasurface (SIM) technology [14], [15]. While [9]–[15] have considered reconfigurable surfaces that passively manipulate the incident EM signal, dynamic metasurface antennas (DMAs) have emerged to actively manipulate how the EM signal is radiated and received [16]. Beyond diagonal DMAs (BD-DMAs) have been recently proposed as an advanced version of DMAs, where tunable interconnections between the meta-atoms enable reconfigurable coupling and hence increase the performance [17].

While analog-domain solutions are particularly appealing

This work has been supported in part by UKRI under Grant EP/Y004086/1, EP/X040569/1, EP/Y037197/1, EP/X04047X/1, EP/Y037243/1.

Matteo Nerini and Bruno Clerckx are with the Department of Electrical and Electronic Engineering, Imperial College London, SW7 2AZ London, U.K. (e-mail: m.nerini20@imperial.ac.uk; b.clerckx@imperial.ac.uk).

for gigantic MIMO beamforming, they commonly suffer from two limitations. First, they typically still rely on digital pre-processing at the transmitter and digital post-processing at the receiver, which could require large hardware and computational complexity in gigantic MIMO. Second, beamforming in the analog domain generally suffers from limited reconfigurability and cannot achieve the same performance as fully digital beamforming. To address both limitations, microwave linear analog computer (MiLAC) has recently emerged as a promising approach for gigantic MIMO systems [18], [19]. A MiLAC is a multiport microwave network made of tunable impedance components, having input and output ports. At the input ports, a signal is applied, which is processed by the MiLAC in the analog domain as it propagates within the microwave network. Thus, at the output ports, the processed signal can be read. Exploiting these analog processing capabilities, we can use a MiLAC at the transmitter side to precode the transmitted symbols by feeding them to the MiLAC input ports through RF chains, and connecting the MiLAC output ports to the transmitting antennas. Similarly, at the receiver side, we can use a MiLAC to combine the received signal by connecting the receiving antennas to the MiLAC input ports and sampling the signal at the MiLAC output ports via RF chains.

By precoding and combining the signal fully in the analog domain, MiLAC offers five distinct advantages for gigantic MIMO in terms of hardware and computational complexity [19]. *First*, it offers the same flexibility as digital beamforming, and hence maximum performance. *Second*, it only requires as many RF chains as the transmitted symbols, i.e., data streams. *Third*, since the signals carried and sampled at the RF chains are the actual symbols, low-resolution ADCs and DACs are sufficient. *Fourth*, it does not require any computation at each symbol time since the symbols are precoded and combined fully in the analog domain. *Fifth*, it can perform zero-forcing beamforming (ZFBB) and minimum mean square error (MMSE) combining with significantly reduced computational complexity, as shown in [19]. In detail, ZFBB and MMSE combining can be executed with a computational complexity growing quadratically with the number of antennas, rather than cubically as in digital MIMO [19].

To analyze the fundamental performance limits of MiLAC, in [18] and [19] it has been assumed that its tunable impedance components can be arbitrarily reconfigured. A more practical design has been considered in [20], where a MiLAC made of lossless and reciprocal tunable impedance components has been considered. Interestingly, even under the lossless and reciprocal constraints, it has been shown that MiLAC-aided beamforming can achieve the same capacity as fully digital beamforming. However, the number of tunable components included in the MiLAC architecture considered in previous work [18], [19], [20] grows quadratically with the number of antennas and streams, which could become prohibitive for very large numbers of antennas and/or streams. To address this issue, in this paper, we propose a novel family of MiLAC architectures with a significantly reduced circuit complexity, which are proven to remain capacity-achieving when made of lossless and reciprocal components. Specifically, the contribution of this paper can be summarized as follows.

*First*, we propose a model of MiLAC based on graph theory. With this model, we represent any MiLAC architecture through a graph, whose vertices correspond to the MiLAC ports and edges correspond to the tunable admittance components interconnecting them. While prior work has focused on fully-connected MiLACs, where every port is interconnected to all other ports, our graph theoretical modeling enables the exploration of different MiLAC architectures, with sparse interconnections and therefore reduced circuit complexity.

*Second*, we characterize a family of MiLAC architectures, named stem-connected MiLACs, which is proven to achieve capacity in point-to-point MIMO systems. Compared to a fully-connected MiLAC, a stem-connected MiLAC has a significantly reduced circuit complexity, measured by the number of tunable admittance components interconnecting its ports. While the circuit complexity of a fully-connected MiLAC is  $\mathcal{O}((N_S + N_T)^2)$ , where  $N_S$  is the number of transmitted streams and  $N_T$  is the number of transmitting antennas, the circuit complexity of a stem-connected MiLAC is  $\mathcal{O}(N_S N_T)$ .

*Third*, we optimize stem-connected MiLACs at both transmitter and receiver sides and demonstrate that they can achieve the capacity for any channel realization. To this end, we first formulate a feasibility check problem whose solution, if it exists, is proven to satisfy a sufficient and necessary condition for achieving capacity. We then solve the obtained problem in closed form, proving that stem-connected MiLACs are capacity-achieving.

*Fourth*, we provide numerical results to support our theoretical findings. Monte Carlo simulations confirm that a stem-connected MiLAC achieves channel capacity for any channel realization, as a fully-connected MiLAC. At the same time, the stem-connected MiLAC architecture offers significantly lower circuit complexity. While the number of tunable admittance components in a fully-connected MiLAC scales quadratically with the number of antennas, it scales only linearly with the number of antennas in a stem-connected MiLAC.

*Organization*: In Section II, we formalize the system model of a MiLAC-aided MIMO system. In Section III, we propose a graph theoretical model of MiLAC architectures. In Section IV, we present a novel family of capacity-achieving MiLAC architectures, named stem-connected MiLACs. In Sections V and VI, we optimize stem-connected MiLACs at the transmitter and the receiver side, respectively, with closed-form solutions proven to achieve capacity. In Section VII, we provide numerical results. Section VIII concludes the paper.

*Notation*: Vectors and matrices are denoted with bold lower and bold upper letters, respectively. Scalars are represented with letters not in bold font.  $\Re\{a\}$ ,  $\Im\{a\}$ , and  $|a|$  refer to the real part, imaginary part, and absolute value of a complex scalar  $a$ , respectively.  $\mathbf{a}^*$ ,  $\mathbf{a}^T$ ,  $\mathbf{a}^H$ ,  $[\mathbf{a}]_i$ , and  $\|\mathbf{a}\|$  refer to the conjugate, transpose, conjugate transpose,  $i$ th element, and  $l_2$ -norm of a vector  $\mathbf{a}$ , respectively.  $\mathbf{A}^*$ ,  $\mathbf{A}^T$ ,  $\mathbf{A}^H$ ,  $[\mathbf{A}]_{i,k}$ ,  $[\mathbf{A}]_{i,:}$ , and  $[\mathbf{A}]_{:,k}$  refer to the conjugate, transpose, conjugate transpose,  $(i, k)$ th element,  $i$ th row, and  $k$ th column of a matrix  $\mathbf{A}$ , respectively.  $[\mathbf{A}]_{\mathcal{I},\mathcal{K}}$  refers to the submatrix of  $\mathbf{A}$  obtained by selecting the rows and columns indexed by the elements of the sets  $\mathcal{I}$  and  $\mathcal{K}$ , respectively.  $\mathbb{R}$  and  $\mathbb{C}$  denote the real and complex number sets, respectively.  $j = \sqrt{-1}$  denotes the

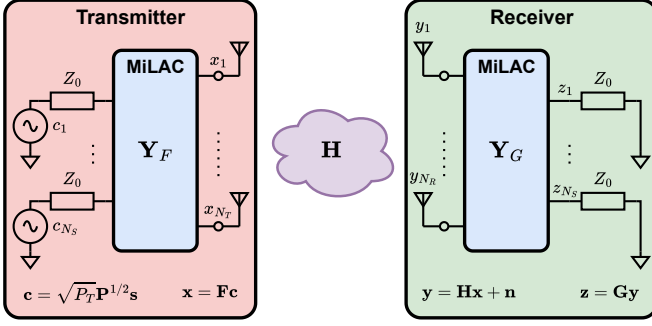


Fig. 1. MiLAC-aided MIMO system model.

imaginary unit.  $\mathbf{I}_N$  and  $\mathbf{0}_N$  denote the identity matrix and the all-zero matrix with dimensions  $N \times N$ , respectively.  $\mathbf{0}_{M \times N}$  denotes the all-zero matrix with dimensions  $M \times N$ .

## II. SYSTEM MODEL

Consider a point-to-point MIMO system aided by a MiLAC at both the transmitter and receiver, as introduced in [20, Section II] and represented in Fig. 1. The  $N_T$ -antenna transmitter sends  $N_S$  symbols (or streams) to the  $N_R$ -antenna receiver, where  $N_S \leq \min\{N_T, N_R\}$ . Following the model in [20, Section II], the signal used for detection at the receiver  $\mathbf{z} \in \mathbb{C}^{N_S \times 1}$  is

$$\mathbf{z} = \sqrt{P_T} \mathbf{G} \mathbf{H} \mathbf{F} \mathbf{P}^{1/2} \mathbf{s} + \mathbf{G} \mathbf{n}, \quad (1)$$

where  $\mathbf{s} \in \mathbb{C}^{N_S \times 1}$  is the symbol vector such that  $\mathbb{E}[\mathbf{s} \mathbf{s}^H] = \mathbf{I}_{N_S}$ ,  $\mathbf{P}^{1/2} \in \mathbb{C}^{N_S \times N_S}$  is the square root of the power allocation matrix given by  $\mathbf{P}^{1/2} = \text{diag}(\sqrt{p_1}, \dots, \sqrt{p_{N_S}})$ , with  $p_s$  denoting the power allocation for the  $s$ th symbol such that  $\sum_{s=1}^{N_S} p_s = 1$ , and  $P_T$  is the transmitted power. In addition,  $\mathbf{F} \in \mathbb{C}^{N_T \times N_S}$  is the precoding matrix implemented by the transmitter-side MiLAC,  $\mathbf{H} \in \mathbb{C}^{N_R \times N_T}$  is the wireless channel, and  $\mathbf{G} \in \mathbb{C}^{N_S \times N_R}$  is the combining matrix implemented by the receiver-side MiLAC. Besides,  $\mathbf{n} \in \mathbb{C}^{N_R \times 1}$  is the additive white Gaussian noise (AWGN) such that  $\mathbb{E}[\mathbf{n} \mathbf{n}^H] = \sigma^2 \mathbf{I}_{N_R}$ , with  $\sigma^2$  denoting the noise power.

According to [19], the precoding matrix  $\mathbf{F}$  is a function of the admittance matrix of the MiLAC at the transmitter  $\mathbf{Y}_F \in \mathbb{C}^{(N_S+N_T) \times (N_S+N_T)}$  and writes as

$$\mathbf{F} = \left[ \left( \frac{\mathbf{Y}_F}{Y_0} + \mathbf{I}_{N_S+N_T} \right)^{-1} \right]_{N_S+\mathcal{N}_T, \mathcal{N}_S}, \quad (2)$$

where  $\mathcal{N}_T = \{1, \dots, N_T\}$  and  $\mathcal{N}_S = \{1, \dots, N_S\}$ <sup>1</sup>. Considering the MiLAC at the transmitter to be composed of a lossless and reciprocal microwave network, its admittance matrix  $\mathbf{Y}_F$  is purely imaginary and symmetric according to microwave network theory [21, Chapter 4], i.e.,  $\mathbf{Y}_F = j\mathbf{B}_F$ , with  $\mathbf{B}_F = \mathbf{B}_F^T$ , where  $\mathbf{B}_F \in \mathbb{R}^{(N_S+N_T) \times (N_S+N_T)}$  is the susceptance matrix of the MiLAC. In alternative to the admittance matrix, the transmitter-side MiLAC can be represented

with its scattering matrix  $\Theta_F \in \mathbb{C}^{(N_S+N_T) \times (N_S+N_T)}$ , related to  $\mathbf{Y}_F$  via

$$\Theta_F = (Y_0 \mathbf{I}_{N_S+N_T} + \mathbf{Y}_F)^{-1} (Y_0 \mathbf{I}_{N_S+N_T} - \mathbf{Y}_F), \quad (3)$$

and the precoding matrix  $\mathbf{F}$  in (2) can be simplified as

$$\mathbf{F} = \frac{1}{2} [\Theta_F]_{N_S+\mathcal{N}_T, \mathcal{N}_S}, \quad (4)$$

as a function of  $\Theta_F$ , equivalently to (2) [20]. In the case of a lossless and reciprocal MiLAC, its scattering matrix is unitary and symmetric, i.e.,  $\Theta_F^H \Theta_F = \mathbf{I}_{N_S+N_T}$ ,  $\Theta_F = \Theta_F^T$  [20].

At the receiver side, the combining matrix  $\mathbf{G}$  is given by

$$\mathbf{G} = \left[ \left( \frac{\mathbf{Y}_G}{Y_0} + \mathbf{I}_{N_R+N_S} \right)^{-1} \right]_{N_R+\mathcal{N}_S, \mathcal{N}_R}, \quad (5)$$

where  $\mathcal{N}_R = \{1, \dots, N_R\}$ , as a function of the admittance matrix of the MiLAC at the receiver  $\mathbf{Y}_G \in \mathbb{C}^{(N_R+N_S) \times (N_R+N_S)}$ . For a lossless and reciprocal MiLAC,  $\mathbf{Y}_G$  is subject to  $\mathbf{Y}_G = j\mathbf{B}_G$ ,  $\mathbf{B}_G = \mathbf{B}_G^T$ , with  $\mathbf{B}_G \in \mathbb{R}^{(N_R+N_S) \times (N_R+N_S)}$  being the susceptance matrix of the MiLAC. Alternatively, we can introduce the scattering matrix of the MiLAC at the receiver  $\Theta_G \in \mathbb{C}^{(N_R+N_S) \times (N_R+N_S)}$  as

$$\Theta_G = (Y_0 \mathbf{I}_{N_R+N_S} + \mathbf{Y}_G)^{-1} (Y_0 \mathbf{I}_{N_R+N_S} - \mathbf{Y}_G), \quad (6)$$

and express the combining matrix  $\mathbf{G}$  as

$$\mathbf{G} = \frac{1}{2} [\Theta_G]_{N_R+\mathcal{N}_S, \mathcal{N}_R}. \quad (7)$$

equivalently to (5) [20], where  $\Theta_G^H \Theta_G = \mathbf{I}_{N_R+N_S}$  and  $\Theta_G = \Theta_G^T$  for a lossless and reciprocal MiLAC.

Given the system model in (1), the achievable rate that can be obtained with MiLAC-aided beamforming is

$$R = \sum_{s=1}^{N_S} \log_2 \left( 1 + \frac{P_T p_s |[\mathbf{G} \mathbf{H} \mathbf{F}]_{s,s}|^2}{P_T \sum_{t \neq s} p_t |[\mathbf{G} \mathbf{H} \mathbf{F}]_{s,t}|^2 + \|[\mathbf{G}]_{s,:}\|^2 \sigma^2} \right), \quad (8)$$

where inter-stream interference is treated as noise since the receiver combines the symbols purely in the analog domain, avoiding further digital processing [20]. By optimally reconfiguring the admittance matrices of the MiLACs  $\mathbf{Y}_F$  and  $\mathbf{Y}_G$  and the power allocations  $p_1, \dots, p_{N_S}$ , the maximum achievable rate, i.e., the capacity, is given by

$$C = \sum_{s=1}^{N_S} \log_2 \left( 1 + \frac{P_T p_s^* \lambda_s}{4\sigma^2} \right), \quad (9)$$

where  $\lambda_s$  is the  $s$ th eigenvalue of  $\mathbf{H} \mathbf{H}^H$  and  $p_s^*$  is the optimal power allocation for the  $s$ th symbol obtained through water-filling, as discussed in [20]<sup>2</sup>.

It has been shown in [20] that the capacity in (9) can be achieved by lossless and reciprocal MiLACs, having tunable admittance components in their multiport microwave networks interconnecting each port to each other. However, the circuit complexity of such MiLACs, defined as the number of tunable admittance components in their microwave networks, grows

<sup>1</sup>We recall that the product  $\mathbf{F} \mathbf{c}$  of the precoding matrix  $\mathbf{F}$  with the power-allocated symbol vector  $\mathbf{c} = \sqrt{P_T} \mathbf{P}^{1/2} \mathbf{s}$  is performed in the analog domain by the MiLAC, which receives in input the signal  $\mathbf{c}$  (see Fig. 1).

<sup>2</sup>Note that we refer to the maximum achievable rate in (8) as the capacity with a slight abuse of terminology, since (8) is strictly speaking the capacity only when  $N_S = \min\{N_T, N_R\}$ .

quadratically with the number of antennas, becoming prohibitive in gigantic MIMO systems. To address this problem, we investigate whether there exist lower-complexity MiLAC architectures still able to achieve the capacity.

### III. GRAPH THEORETICAL MODELING OF MiLAC

In this section, we model MiLAC architectures as graphs, inspired by the graph theoretical modeling of BD-RIS introduced in [22]. This modeling shows that numerous MiLAC architectures are available to balance flexibility and circuit complexity.

A MiLAC has been introduced in [18] as a multiport microwave network made of tunable admittance components interconnecting the ports to ground and to each other. Considering a MiLAC with  $N_V$  ports, we denote as  $Y_{n,n} \in \mathbb{C}$  the admittance connecting port  $n$  to ground, for  $n = 1, \dots, N_V$ , and as  $Y_{m,n} \in \mathbb{C}$  the admittance interconnecting ports  $m$  and  $n$ ,  $\forall m \neq n$ . As a function of these tunable admittance components, the admittance matrix of the MiLAC  $\mathbf{Y} \in \mathbb{C}^{N_V \times N_V}$  writes as

$$[\mathbf{Y}]_{m,n} = \begin{cases} -Y_{m,n} & m \neq n \\ \sum_{k=1}^{N_V} Y_{k,n} & m = n \end{cases}, \quad (10)$$

for  $m, n = 1, \dots, N_V$  [18]. In a MiLAC where the ports are all interconnected to each other, i.e., including all admittance components  $Y_{m,n}$ , for  $m, n = 1, \dots, N_V$ ,  $\mathbf{Y}$  can be any arbitrary matrix following (10). In the case of lossless and reciprocal admittance components,  $\mathbf{Y}$  can be any arbitrary imaginary symmetric matrix, as considered in Section II. Nevertheless, besides this MiLAC architecture where the ports are all interconnected to each other, it is also possible to design MiLAC architectures including only a reduced number of interconnections between ports, and hence having lower circuit complexity. If ports  $m$  and  $n$  are not interconnected,  $Y_{m,n}$  is an open circuit, i.e., it is forced to zero. As a consequence of  $Y_{m,n} = 0$ , also the  $(m,n)$ th element of  $\mathbf{Y}$  is forced to zero according to (10), limiting the flexibility of the resulting MiLAC. This observation enables us to design numerous MiLAC architectures that strike a balance between flexibility and circuit complexity.

To formally characterize all possible MiLAC architectures, we represent the circuit topology of any  $N_V$ -port MiLAC through a simple undirected graph  $\mathcal{G} = (\mathcal{V}, \mathcal{E})$ , where  $\mathcal{V}$  and  $\mathcal{E}$  are its vertex set and edge set, respectively [23]. The set  $\mathcal{V}$  is constituted by the indexes of the ports of the MiLAC, i.e.,

$$\mathcal{V} = \{V_1, \dots, V_{N_V}\}, \quad (11)$$

where  $N_V$  denotes the number of MiLAC ports, which is  $N_V = N_S + N_T$  or  $N_V = N_R + N_S$  for a transmitter- or receiver-side MiLAC, respectively. The set  $\mathcal{E}$  is defined as

$$\mathcal{E} = \{(V_n, V_m) \mid V_n, V_m \in \mathcal{V}, Y_{n,m} \neq 0, n \neq m\}, \quad (12)$$

meaning that there is an edge between vertices  $V_m$  and  $V_n$  if and only if there is a tunable admittance component interconnecting ports  $m$  and  $n$ . In a lossless and reciprocal MiLAC with associated graph  $\mathcal{G} = (\mathcal{V}, \mathcal{E})$ , the admittance

matrix is therefore subject to  $\mathbf{Y} = j\mathbf{B}$ , with the susceptance matrix  $\mathbf{B}$  fulfilling  $\mathbf{B} = \mathbf{B}^T$  and  $\mathbf{B} \in \mathcal{B}_{\mathcal{G}}$ , where

$$\mathcal{B}_{\mathcal{G}} = \left\{ \mathbf{B} \in \mathbb{R}^{N_V \times N_V} \mid [\mathbf{B}]_{n,m} = 0, \forall n \neq m, (V_n, V_m) \notin \mathcal{E} \right\}, \quad (13)$$

indicating that the  $(m,n)$ th element of  $\mathbf{Y}$  is forced to zero if ports  $m$  and  $n$  are not interconnected by a tunable admittance. Besides, the circuit complexity of such a MiLAC, defined as the number of tunable admittance components, is given by  $N_C = N_V + N_E$ , where  $N_E$  denotes the cardinality of  $\mathcal{E}$ , since there are  $N_V$  tunable admittance components connecting each port to ground and  $N_E$  components interconnecting the ports.

The MiLAC architecture considered in previous works [18], [19], [20], that we denote as fully-connected MiLAC, has an associated graph  $\mathcal{G}$  that is the complete graph on  $N_V$  vertices. Therefore, in this case we have  $\mathcal{B}_{\mathcal{G}} = \mathbb{R}^{N_V \times N_V}$ , yielding maximum flexibility, and  $N_E = N_V(N_V - 1)/2$  edges in  $\mathcal{G}$ , yielding a circuit complexity of

$$N_C^{\text{Fully}} = \frac{N_V(N_V + 1)}{2}. \quad (14)$$

For a transmitter-side MiLAC, where  $N_V = N_S + N_T$ , we have a circuit complexity of

$$N_C^{\text{Fully}} = \frac{(N_S + N_T)(N_S + N_T + 1)}{2}, \quad (15)$$

growing with  $\mathcal{O}((N_S + N_T)^2)$ , i.e., quadratically with the number of antennas  $N_T$ . A similar discussion holds for a MiLAC at the receiver and, by replacing  $N_T$  with  $N_R$  in (15), we obtain that its complexity scales with  $\mathcal{O}((N_S + N_R)^2)$ , i.e., quadratically with  $N_R$ . Although the fully-connected MiLAC offers the highest flexibility, corresponding to the largest set  $\mathcal{B}_{\mathcal{G}}$ , it also incurs the highest circuit complexity, which scales quadratically with the number of antennas. This motivates the design of alternative MiLAC architectures with reduced circuit complexity that ideally do not significantly compromise the achievable rate despite their reduced flexibility.

### IV. CAPACITY-ACHIEVING MiLAC ARCHITECTURES

We have introduced a graph theoretical model for MiLAC and showed that numerous MiLAC architectures are available to balance flexibility and circuit complexity. In this section, we propose a family of MiLAC architectures proven to be capacity-achieving despite their highly reduced circuit complexity.

#### A. Definition of Capacity-Achieving MiLAC Architectures

We begin by recalling under which conditions we can achieve capacity in a MiLAC-aided system, and providing a formal definition of capacity-achieving MiLAC architecture. According to [20], the capacity in (9) can be achieved by setting the scattering matrix of the transmitter-side MiLAC  $\Theta_F$  such that  $[\Theta_F]_{N_S + N_T, N_S} = \bar{\mathbf{V}}$ , where  $\bar{\mathbf{V}} \in \mathbb{C}^{N_T \times N_S}$  contains the first  $N_S$  right singular vectors of  $\mathbf{H}$ , and the scattering matrix of the receiver-side MiLAC  $\Theta_G$  such that  $[\Theta_G]_{N_R + N_S, N_R} = \bar{\mathbf{U}}^H$ , where  $\bar{\mathbf{U}} \in \mathbb{C}^{N_R \times N_S}$  contains the first  $N_S$  left singular vectors of  $\mathbf{H}$ .

Following these capacity-achieving conditions, a MiLAC at the transmitter is defined as capacity-achieving if its scattering matrix  $\Theta_F$  can be reconfigured such that  $[\Theta_F]_{N_S+N_T, N_S} = \bar{\mathbf{V}}$ , for any given matrix  $\bar{\mathbf{V}} \in \mathbb{C}^{N_T \times N_S}$  having orthogonal columns with unit  $\ell_2$ -norm. This means that a transmitter-side MiLAC is capacity-achieving if the first  $N_S$  columns of its scattering matrix can be reconfigured to  $[\mathbf{0}_{N_S}, \bar{\mathbf{V}}^T]^T$ , for any possible  $\bar{\mathbf{V}}$ . Formally,  $\Theta_F$  must satisfy

$$\Theta_F \begin{bmatrix} \mathbf{I}_{N_S} \\ \mathbf{0}_{N_T \times N_S} \end{bmatrix} = \begin{bmatrix} \mathbf{0}_{N_S} \\ \bar{\mathbf{V}} \end{bmatrix}, \quad (16)$$

for any possible  $\bar{\mathbf{V}}$ , where the product  $\Theta_F[\mathbf{I}_{N_S}, \mathbf{0}_{N_S \times N_T}]^T$  returns the first  $N_S$  columns of  $\Theta_F$ . We have shown in [20] that a fully-connected MiLAC (lossless and reciprocal) is capacity-achieving. However, when considering different MiLAC architectures with a reduced number of admittance components, their susceptance matrix  $\mathbf{B}_F$  must be such that  $\mathbf{B}_F \in \mathcal{B}_G$  and cannot be an arbitrary symmetric matrix. As a consequence, the scattering matrix  $\Theta_F$ , which is a function of  $\mathbf{Y}_F = j\mathbf{B}_F$  as in (3), cannot be an arbitrary unitary symmetric matrix, and condition (16) might not be achievable for any value of  $\bar{\mathbf{V}}$ .

Similarly, a MiLAC at the receiver is defined as capacity-achieving if its scattering matrix  $\Theta_G$  can be reconfigured such that  $[\Theta_G]_{N_R+N_S, N_R} = \bar{\mathbf{U}}^H$ , for any  $\bar{\mathbf{U}} \in \mathbb{C}^{N_R \times N_S}$  having orthogonal columns with unit  $\ell_2$ -norm. In other words, a receiver-side MiLAC is capacity-achieving if the last  $N_S$  rows of its scattering matrix can be reconfigured to  $[\bar{\mathbf{U}}^H, \mathbf{0}_{N_S}]$ , for any possible  $\bar{\mathbf{U}}$ , or, equivalently, the last  $N_S$  columns of its scattering matrix can be reconfigured to  $[\bar{\mathbf{U}}^H, \mathbf{0}_{N_S}]^T$ , given the symmetry of  $\Theta_G$ . More precisely,  $\Theta_G$  must satisfy

$$\Theta_G \begin{bmatrix} \mathbf{0}_{N_T \times N_S} \\ \mathbf{I}_{N_S} \end{bmatrix} = \begin{bmatrix} \bar{\mathbf{U}}^* \\ \mathbf{0}_{N_S} \end{bmatrix}, \quad (17)$$

for any possible  $\bar{\mathbf{U}}$ , where the product  $\Theta_G[\mathbf{0}_{N_S \times N_T}, \mathbf{I}_{N_S}]^T$  returns the last  $N_S$  columns of  $\Theta_G$ . As discussed for the transmitter-side MiLAC, a fully-connected MiLAC (lossless and reciprocal) is capacity-achieving [20]. However, other MiLAC architectures with a reduced number of admittance components, and hence reduced flexibility, could not be capacity-achieving.

### B. A Family of Capacity-Achieving MiLAC Architectures

As the circuit complexity of a fully-connected MiLAC becomes prohibitive when the number of antennas grows high, we are interested in alternative capacity-achieving MiLAC architectures with a reduced circuit complexity. Before providing a sufficient condition for a MiLAC architecture to be capacity-achieving, we introduce the concept of center graph.

**Definition 1.** A center graph with center size  $Q$  is a graph that contains  $Q$  vertices, denoted as central vertices, each connected to all other vertices, while the remaining vertices are only connected to the central vertices.

As an illustrative example, we report a center graph on  $N$  vertices with center size  $Q = 4$  in Fig. 2, where the central vertices are  $V_1, V_2, V_3$ , and  $V_4$ . We denote a MiLAC with

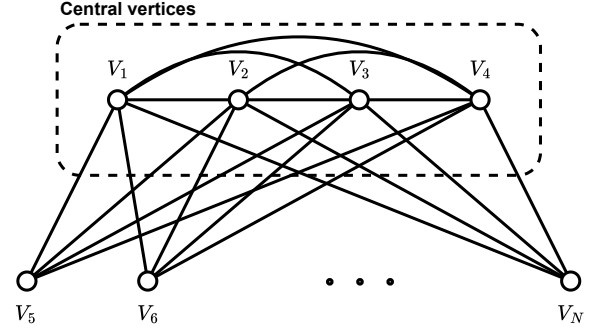


Fig. 2. Center graph with center size  $Q = 4$ .

associated graph being a center graph as a stem-connected MiLAC, following the terminology introduced in BD-RIS literature [24], [25].

Based on this definition of center graph, the following proposition gives a sufficient condition for a transmitter-side MiLAC architecture to satisfy (16) for any  $\bar{\mathbf{V}}$ , i.e., for being capacity-achieving.

**Proposition 1.** A transmitter-side MiLAC with associated graph  $\mathcal{G}$  is capacity-achieving if  $\mathcal{G}$  is a center graph with center size  $Q = 2N_S - 1$  and its central vertices include the  $N_S$  vertices corresponding to the input ports of the MiLAC.

*Proof.* This proposition is proven in Section V, where we optimize MiLAC architectures satisfying this sufficient condition with a closed-form solution that fulfills (16) for any  $\bar{\mathbf{V}}$ .  $\square$

Fig. 3(a) shows the graph corresponding to a stem-connected MiLAC at the transmitter, having center size  $Q = 2N_S - 1$ . Note that the central vertices include all the  $N_S$  vertices associated with the input ports (in red), i.e.,  $V_1, \dots, V_{N_S}$ . In addition, the central vertices also include  $N_S - 1$  vertices associated with any  $N_S - 1$  output ports (in green), which are  $V_{N_S+1}, \dots, V_{2N_S-1}$  in Fig. 3(a). Since in this graph the first  $2N_S - 1$  vertices are connected to all other vertices, the susceptance matrix of the corresponding MiLAC is constrained as  $\mathbf{B}_F \in \mathcal{B}_F$ , where

$$\mathcal{B}_F = \left\{ \mathbf{B} \in \mathbb{R}^{(N_S+N_T) \times (N_S+N_T)} \mid [\mathbf{B}]_{n,m} = 0, \forall n \neq m, \right. \\ \left. n > 2N_S - 1, m > 2N_S - 1 \right\}, \quad (18)$$

meaning that only the elements in the first  $2N_S - 1$  rows and columns and in the main diagonal are tunable. A representation of such a matrix  $\mathbf{B}_F$  is reported in Fig. 3(b), where the tunable elements are highlighted in gray. Note that, although in Fig. 3(a) we have selected the output ports  $V_{N_S+1}, \dots, V_{2N_S-1}$  to be connected to all the others, any set of  $N_S - 1$  output ports could be chosen. Accordingly, the corresponding  $N_S - 1$  rows and columns of the matrix  $\mathbf{B}_F$  in Fig. 3(b) will be tunable.

As discussed for a transmitter-side MiLAC, the following proposition gives a sufficient condition for a receiver-side MiLAC architecture to satisfy (17) for any  $\bar{\mathbf{U}}$ , i.e., for being capacity-achieving.

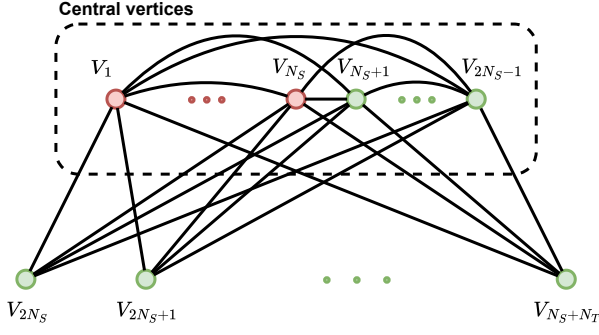
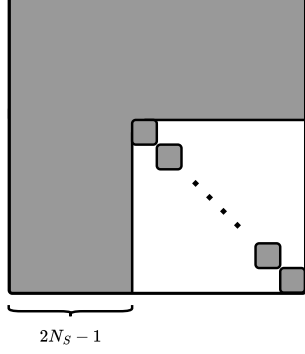
(a) Center graph with center size  $Q = 2N_S - 1$ .(b) Susceptance matrix  $\mathbf{B}_F$ .

Fig. 3. (a) Graph and (b) susceptance matrix (with tunable elements in gray) of a capacity-achieving stem-connected MiLAC at the transmitter.

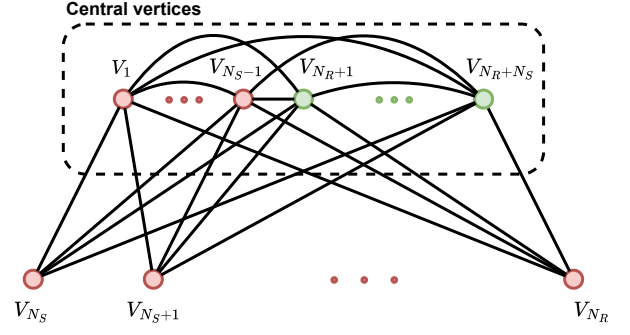
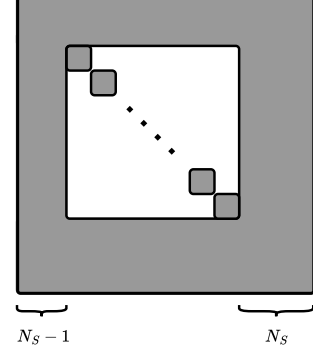
(a) Center graph with center size  $Q = 2N_S - 1$ .(b) Susceptance matrix  $\mathbf{B}_G$ .

Fig. 4. (a) Graph and (b) susceptance matrix (with tunable elements in gray) of a capacity-achieving stem-connected MiLAC at the receiver.

**Proposition 2.** A receiver-side MiLAC with associated graph  $\mathcal{G}$  is capacity-achieving if  $\mathcal{G}$  is a center graph with center size  $Q = 2N_S - 1$  and its central vertices include the  $N_S$  vertices corresponding to the output ports of the MiLAC.

*Proof.* Similar to Proof of Proposition 1, we prove this proposition in Section VI by optimizing these MiLAC architectures with a closed-form solution that achieves capacity.  $\square$

Fig. 4(a) shows the graph corresponding to a stem-connected MiLAC at the receiver, with center size  $Q = 2N_S - 1$ . The central vertices include all the  $N_S$  vertices associated with the output ports (in green), i.e.,  $V_{NR+1}, \dots, V_{NR+NS}$ . In addition, the central vertices also include  $N_S - 1$  vertices associated with any  $N_S - 1$  input ports (in red), namely  $V_1, \dots, V_{NS-1}$  in Fig. 4(a). Since in this graph the first  $N_S - 1$  and last  $N_S$  vertices are connected to all other vertices, the susceptance matrix of the corresponding MiLAC is constrained as  $\mathbf{B}_G \in \mathcal{B}_G$ , where

$$\mathcal{B}_G = \left\{ \mathbf{B} \in \mathbb{R}^{(NR+NS) \times (NR+NS)} \mid [\mathbf{B}]_{n,m} = 0, \forall n \neq m, \right. \\ \left. N_S - 1 < n \leq N_R, N_S - 1 < m \leq N_R \right\}, \quad (19)$$

meaning that only the elements in the first  $N_S - 1$  and last  $N_S$  rows and columns and in the main diagonal are tunable. A representation of such a matrix  $\mathbf{B}_G$  is reported in Fig. 4(b), where the tunable elements are highlighted in gray. Note that, although in Fig. 4(a) we have selected the input ports  $V_1, \dots, V_{NS-1}$  to be connected to all the others, any set

of  $N_S - 1$  input ports could be chosen<sup>3</sup>. Accordingly, the corresponding  $N_S - 1$  rows and columns of the matrix  $\mathbf{B}_G$  in Fig. 4(b) will be tunable.

A stem-connected MiLAC can achieve capacity with a significantly reduced circuit complexity compared to a fully-connected MiLAC. To quantify the circuit complexity of a stem-connected MiLAC, we recall that its complexity is given by  $N_C = N_V + N_E$ , where  $N_V$  and  $N_E$  are the number of vertices and edges of its associated graph, which is a center graph with center size  $Q$ . Since the number of edges in a center graph on  $N_V$  vertices and having center size  $Q$  is  $N_E = Q(Q - 1)/2 + Q(N_V - Q)$ , the complexity of a stem-connected MiLAC is given by

$$N_C^{\text{Stem}} = N_V + \frac{Q(Q - 1)}{2} + Q(N_V - Q) \quad (20)$$

$$= \frac{(Q + 1)(2N_V - Q)}{2}. \quad (21)$$

Thus, in the case of a capacity-achieving stem-connected MiLAC at the transmitter, we can substitute  $N_V = N_S + N_T$  and  $Q = 2N_S - 1$  into (21) and obtain

$$N_C^{\text{Stem}} = N_S(2N_T + 1), \quad (22)$$

growing with  $\mathcal{O}(N_S N_T)$ , i.e., linearly with the number of antennas  $N_T$ . A similar discussion holds for a receiver-side MiLAC and, by replacing  $N_T$  in (22) with  $N_R$ , we obtain

<sup>3</sup>We have selected the input ports  $V_1, \dots, V_{NS-1}$  because the optimization of such a receiver-side MiLAC is analogous to that of the transmitter-side MiLAC shown in Fig. 3, as it will be clarified in Section VI.

TABLE I  
FULLY- AND STEM-CONNECTED MiLAC ARCHITECTURES.

MiLAC architecture	Associated graph	Circuit complexity*	Description*
Fully-connected MiLAC	Complete graph	$N_C^{\text{Fully}} = (N_S + N_T)(N_S + N_T + 1)/2$	All $N_S + N_T$ MiLAC ports are connected to each other
Stem-connected MiLAC	Center graph	$N_C^{\text{Stem}} = N_S(2N_T + 1)$	Only $2N_S - 1$ MiLAC ports are connected to all the others

\* For the stem-connected MiLAC, we consider  $Q = 2N_S - 1$ . The same discussion applies to a receiver-side MiLAC by replacing  $N_T$  with  $N_R$ .

that its circuit complexity scales with  $\mathcal{O}(N_S N_R)$ , i.e., linearly with  $N_R$ . We summarize the main properties of fully- and stem-connected MiLACs in Tab. I.

**Remark 1.** *The capacity-achieving stem-connected MiLAC architectures introduced in Propositions 1 and 2 have a center size  $Q = 2N_S - 1$ . Note that such a value of the center size is aligned with the center size of optimal stem-connected RIS architectures proposed in [24] and analyzed in [25]. In detail, a sufficient condition for stem-connected RISs to achieve maximum performance is to have a center size  $Q = 2K - 1$ , with  $K$  denoting the degrees of freedom, or multiplexing gain, of the RIS-aided MIMO channel, as observed in [24] and proven in [25, Corollary 2]. Similarly, the capacity-achieving stem-connected MiLACs in Propositions 1 and 2 have a center size  $Q = 2N_S - 1$ , as the number of streams  $N_S$  is the multiplexing gain of the MiLAC-aided MIMO channel.*

**Remark 2.** *The capacity-achieving stem-connected MiLAC architectures in Proposition 1 have associated graphs including the  $N_S$  vertices corresponding to the input MiLAC ports within their central vertices. Likewise, the MiLAC architectures in Proposition 2 have associated graphs including the  $N_S$  vertices corresponding to the output MiLAC ports within their central vertices. Note that this constraint is imposed since it is required by our capacity-achieving closed-form solutions, as it will be clarified in Sections V and VI. Thus, this constraint is not proven to be necessary to achieve capacity.*

## V. OPTIMIZATION OF CAPACITY-ACHIEVING TRANSMITTER-SIDE MiLAC ARCHITECTURES

We have introduced stem-connected MiLAC architectures and claimed in Proposition 1 that they are capacity-achieving. In this section, we prove Proposition 1 by optimizing a stem-connected MiLAC at the transmitter through a closed-form that achieves capacity. To simplify the notation, only in this section, we denote the scattering, admittance, and susceptance matrices of the considered MiLAC at the transmitter as  $\Theta$ ,  $\mathbf{Y}$ , and  $\mathbf{B}$  instead of  $\Theta_F$ ,  $\mathbf{Y}_F$ , and  $\mathbf{B}_F$ .

### A. Reformulation of the Capacity-Achieving Condition

By recalling that  $\Theta$  can be expressed as a function of the admittance matrix  $\mathbf{Y} = j\mathbf{B}$  as in (3), the capacity-achieving condition in (16) can be reformulated as

$$(Y_0 \mathbf{I} - j\mathbf{B}) \begin{bmatrix} \mathbf{I}_{N_S} \\ \mathbf{0}_{N_T \times N_S} \end{bmatrix} = (Y_0 \mathbf{I} + j\mathbf{B}) \begin{bmatrix} \mathbf{0}_{N_S} \\ \mathbf{V} \end{bmatrix}, \quad (23)$$

as a function of  $\mathbf{B}$  rather than  $\Theta$ . After algebraic computations, from (23) we obtain

$$j\mathbf{B} \begin{bmatrix} \mathbf{I}_{N_S} \\ \mathbf{V} \end{bmatrix} = Y_0 \begin{bmatrix} \mathbf{I}_{N_S} \\ -\mathbf{V} \end{bmatrix}, \quad (24)$$

or, equivalently,

$$j \begin{bmatrix} \mathbf{I}_{N_S} & \mathbf{V}^T \end{bmatrix} \mathbf{B} = Y_0 \begin{bmatrix} \mathbf{I}_{N_S} & -\mathbf{V}^T \end{bmatrix}, \quad (25)$$

since  $\mathbf{B}$  is symmetric. The condition in (25) is a linear matrix equation with real unknowns, i.e., the entries of the real matrix  $\mathbf{B}$ , and complex coefficients, i.e., the entries of the complex matrices  $j \begin{bmatrix} \mathbf{I}_{N_S} & \mathbf{V}^T \end{bmatrix}$  and  $Y_0 \begin{bmatrix} \mathbf{I}_{N_S} & -\mathbf{V}^T \end{bmatrix}$ . To transform (25) into a linear matrix equation with real coefficients, we equivalently rewrite it as

$$\begin{bmatrix} \Re \{ j \begin{bmatrix} \mathbf{I}_{N_S} & \mathbf{V}^T \end{bmatrix} \} \\ \Im \{ j \begin{bmatrix} \mathbf{I}_{N_S} & \mathbf{V}^T \end{bmatrix} \} \end{bmatrix} \mathbf{B} = \begin{bmatrix} \Re \{ Y_0 \begin{bmatrix} \mathbf{I}_{N_S} & -\mathbf{V}^T \end{bmatrix} \} \\ \Im \{ Y_0 \begin{bmatrix} \mathbf{I}_{N_S} & -\mathbf{V}^T \end{bmatrix} \} \end{bmatrix}, \quad (26)$$

which can be expressed more concisely as

$$\begin{bmatrix} \mathbf{0}_{N_S} & -\Im \{ \mathbf{V} \}^T \\ \mathbf{I}_{N_S} & \Re \{ \mathbf{V} \}^T \end{bmatrix} \mathbf{B} = Y_0 \begin{bmatrix} \mathbf{I}_{N_S} & -\Re \{ \mathbf{V} \}^T \\ \mathbf{0}_{N_S} & -\Im \{ \mathbf{V} \}^T \end{bmatrix}. \quad (27)$$

To find a matrix  $\mathbf{B}$  satisfying (27), we partition  $\mathbf{B}$  as

$$\mathbf{B} = \begin{bmatrix} \mathbf{B}_{11} & \mathbf{B}_{12} \\ \mathbf{B}_{21} & \mathbf{B}_{22} \end{bmatrix}, \quad (28)$$

where  $\mathbf{B}_{11} \in \mathbb{R}^{N_S \times N_S}$ ,  $\mathbf{B}_{12} \in \mathbb{R}^{N_S \times N_T}$ ,  $\mathbf{B}_{21} \in \mathbb{R}^{N_T \times N_S}$ , and  $\mathbf{B}_{22} \in \mathbb{R}^{N_T \times N_T}$ . Thus, by introducing  $\mathbf{R} \in \mathbb{R}^{N_S \times N_T}$  and  $\mathbf{J} \in \mathbb{R}^{N_S \times N_T}$  as  $\mathbf{R} = \Re \{ \mathbf{V} \}^T$  and  $\mathbf{J} = \Im \{ \mathbf{V} \}^T$  to alleviate the notation, (27) becomes

$$\begin{bmatrix} \mathbf{0}_{N_S} & -\mathbf{J} \\ \mathbf{I}_{N_S} & \mathbf{R} \end{bmatrix} \begin{bmatrix} \mathbf{B}_{11} & \mathbf{B}_{12} \\ \mathbf{B}_{21} & \mathbf{B}_{22} \end{bmatrix} = Y_0 \begin{bmatrix} \mathbf{I}_{N_S} & -\mathbf{R} \\ \mathbf{0}_{N_S} & -\mathbf{J} \end{bmatrix}. \quad (29)$$

To formalize the constraints on the blocks  $\mathbf{B}_{11}$ ,  $\mathbf{B}_{12}$ ,  $\mathbf{B}_{21}$ , and  $\mathbf{B}_{22}$ , we assume with no loss of generality that the considered stem-connected MiLAC has the  $N_S - 1$  output ports  $V_{N_S+1}, \dots, V_{2N_S-1}$  connected to all the others, as Fig. 3(a). Accordingly, we have  $\mathbf{B} \in \mathcal{B}_F$ , where  $\mathcal{B}_F$  is given by (18). This means that the only constraints on  $\mathbf{B}_{11}$ ,  $\mathbf{B}_{12}$ , and  $\mathbf{B}_{21}$  are  $\mathbf{B}_{11} = \mathbf{B}_{11}^T$  and  $\mathbf{B}_{21} = \mathbf{B}_{12}^T$  (due to the symmetry of  $\mathbf{B}$ , and since the  $N_S$  input ports of the MiLAC are connected to all the others as required by Proposition 1), while  $\mathbf{B}_{22}$  satisfies  $\mathbf{B}_{22} = \mathbf{B}_{22}^T$  and  $\mathbf{B}_{22} \in \mathcal{B}_{22}$ , where

$$\mathcal{B}_{22} = \left\{ \mathbf{B} \in \mathbb{R}^{N_T \times N_T} \mid [\mathbf{B}]_{n,m} = 0, \forall n \neq m, \right. \\ \left. n > N_S - 1, m > N_S - 1 \right\}. \quad (30)$$



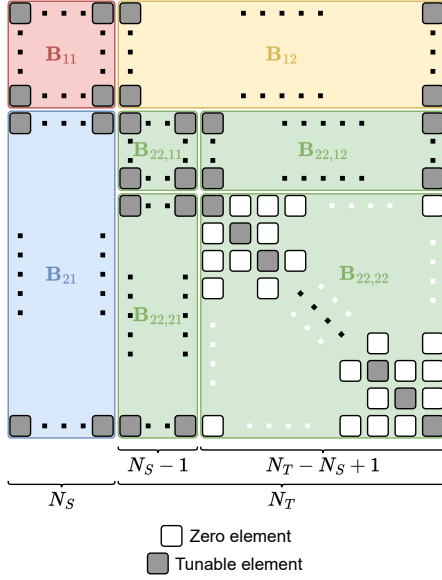


Fig. 5. Admittance matrix  $\mathbf{B}$  of a stem-connected MiLAC at the transmitter partitioned into seven matrices, where  $\mathbf{B}_{22,22}$  is diagonal.

As a result, the problem of optimizing a stem-connected MiLAC through a capacity-achieving solution can be formalized as a feasibility check problem, where we need to find a valid  $\mathbf{B}$  partitioned as in (28) whose blocks satisfy the capacity-achieving condition (29). Formally, we need to solve

$$\text{find } \mathbf{B}_{11}, \mathbf{B}_{12}, \mathbf{B}_{21}, \mathbf{B}_{22} \quad (31)$$

$$\text{s.t. } \mathbf{B}_{11} = \mathbf{B}_{11}^T, \mathbf{B}_{21} = \mathbf{B}_{12}^T, \mathbf{B}_{22} = \mathbf{B}_{22}^T, \quad (32)$$

$$\mathbf{B}_{22} \in \mathcal{B}_{22}, \quad (33)$$

$$\mathbf{J}\mathbf{B}_{21} = -Y_0\mathbf{I}_{N_S}, \quad (34)$$

$$\mathbf{J}\mathbf{B}_{22} = Y_0\mathbf{R}, \quad (35)$$

$$\mathbf{B}_{11} + \mathbf{R}\mathbf{B}_{21} = \mathbf{0}_{N_S}, \quad (36)$$

$$\mathbf{B}_{12} + \mathbf{R}\mathbf{B}_{22} = -Y_0\mathbf{J}, \quad (37)$$

where (32) and (33) follow from the constraints on  $\mathbf{B}$ , and (34)-(37) follow from the capacity-achieving condition (29). In the following subsections, we solve (31)-(37) by first finding a valid block  $\mathbf{B}_{22}$  fulfilling (35), and then finding valid blocks  $\mathbf{B}_{11}$ ,  $\mathbf{B}_{12}$ , and  $\mathbf{B}_{21}$  fulfilling the other constraints in (31)-(37).

### B. Block $\mathbf{B}_{22}$

We first find the block  $\mathbf{B}_{22}$  subject to  $\mathbf{B}_{22} = \mathbf{B}_{22}^T$  and  $\mathbf{B}_{22} \in \mathcal{B}_{22}$  by solving (35). To this end, we conveniently partition the matrix  $\mathbf{B}_{22}$  as

$$\mathbf{B}_{22} = \begin{bmatrix} \mathbf{B}_{22,11} & \mathbf{B}_{22,12} \\ \mathbf{B}_{22,21} & \mathbf{B}_{22,22} \end{bmatrix}, \quad (38)$$

where  $\mathbf{B}_{22,11} \in \mathbb{R}^{(N_S-1) \times (N_S-1)}$  is symmetric,  $\mathbf{B}_{22,12} \in \mathbb{R}^{(N_S-1) \times (N_T-N_S+1)}$  and  $\mathbf{B}_{22,21} \in \mathbb{R}^{(N_T-N_S+1) \times (N_S-1)}$  are such that  $\mathbf{B}_{22,21} = \mathbf{B}_{22,12}^T$ , and  $\mathbf{B}_{22,22} \in \mathbb{R}^{(N_T-N_S+1) \times (N_T-N_S+1)}$  is diagonal since  $\mathbf{B}_{22} \in \mathcal{B}_{22}$ . Note that by substituting (38) into (28), we obtain that the matrix  $\mathbf{B}$  is partitioned into a total of seven matrices, as graphically represented in Fig. 5.

By considering the partition in (38) and the partitions  $\mathbf{R} = [\mathbf{R}_1, \mathbf{R}_2]$ , with  $\mathbf{R}_1 \in \mathbb{R}^{N_S \times (N_S-1)}$  and  $\mathbf{R}_2 \in \mathbb{R}^{N_S \times (N_T-N_S+1)}$  and  $\mathbf{J} = [\mathbf{J}_1, \mathbf{J}_2]$ , with  $\mathbf{J}_1 \in \mathbb{R}^{N_S \times (N_S-1)}$  and  $\mathbf{J}_2 \in \mathbb{R}^{N_S \times (N_T-N_S+1)}$ , (35) can be rewritten as

$$\begin{bmatrix} \mathbf{J}_1 & \mathbf{J}_2 \end{bmatrix} \begin{bmatrix} \mathbf{B}_{22,11} & \mathbf{B}_{22,12} \\ \mathbf{B}_{22,21} & \mathbf{B}_{22,22} \end{bmatrix} = Y_0 [\mathbf{R}_1 \quad \mathbf{R}_2], \quad (39)$$

which is equivalent to a system of two linear matrix equations

$$\begin{cases} \mathbf{J}_1 \mathbf{B}_{22,11} + \mathbf{J}_2 \mathbf{B}_{22,21} = Y_0 \mathbf{R}_1, \\ \mathbf{J}_1 \mathbf{B}_{22,12} + \mathbf{J}_2 \mathbf{B}_{22,22} = Y_0 \mathbf{R}_2. \end{cases} \quad (40)$$

In the following, we find the values for the blocks of  $\mathbf{B}_{22}$  fulfilling this system of equations. We first set the blocks  $\mathbf{B}_{22,12}$ ,  $\mathbf{B}_{22,21}$ , and  $\mathbf{B}_{22,22}$ , and then optimize  $\mathbf{B}_{22,11}$  accordingly.

1) *Blocks  $\mathbf{B}_{22,12}$ ,  $\mathbf{B}_{22,21}$ , and  $\mathbf{B}_{22,22}$ :* Denote as  $\mathbf{r}_i \in \mathbb{R}^{N_S \times 1}$  the  $i$ th column of  $\mathbf{R}$  and as  $\mathbf{j}_i \in \mathbb{R}^{N_S \times 1}$  the  $i$ th column of  $\mathbf{J}$ , for  $i = 1, \dots, N_T$ . Thus, we claim that the  $i$ th diagonal element of the diagonal matrix  $\mathbf{B}_{22,22}$  is given by

$$[\mathbf{B}_{22,22}]_{i,i} = Y_0 \left[ [\mathbf{J}_1, \mathbf{j}_{N_S-1+i}]^{-1} \mathbf{r}_{N_S-1+i} \right]_{N_S}, \quad (42)$$

for  $i = 1, \dots, N_T - N_S + 1$ . In addition, we claim that the  $(j, i)$ th element of  $\mathbf{B}_{22,12}$  is given by

$$[\mathbf{B}_{22,12}]_{j,i} = Y_0 \left[ [\mathbf{J}_1, \mathbf{j}_{N_S-1+i}]^{-1} \mathbf{r}_{N_S-1+i} \right]_j, \quad (43)$$

for  $j = 1, \dots, N_S - 1$  and  $i = 1, \dots, N_T - N_S + 1$ . These claims can be immediately verified by checking that (42) and (43) satisfy (41), i.e.,

$$[\mathbf{J}_1 \mathbf{B}_{22,12} + \mathbf{J}_2 \mathbf{B}_{22,22}]_{j,i} = Y_0 [\mathbf{R}_2]_{j,i}, \quad (44)$$

for  $j = 1, \dots, N_S$  and  $i = 1, \dots, N_T - N_S + 1$ . By substituting (42) and (43) into the left side of (44), we have

$$\begin{aligned} [\mathbf{J}_1 \mathbf{B}_{22,12} + \mathbf{J}_2 \mathbf{B}_{22,22}]_{j,i} &= [\mathbf{J}_1 \mathbf{B}_{22,12}]_{j,i} + [\mathbf{J}_2 \mathbf{B}_{22,22}]_{j,i} \\ &= Y_0 [\mathbf{J}_1]_{j,:} \left[ [\mathbf{J}_1, \mathbf{j}_{N_S-1+i}]^{-1} \mathbf{r}_{N_S-1+i} \right]_{1:N_S-1} \\ &\quad + Y_0 [\mathbf{J}_2]_{j,i} \left[ [\mathbf{J}_1, \mathbf{j}_{N_S-1+i}]^{-1} \mathbf{r}_{N_S-1+i} \right]_{N_S} \\ &= Y_0 [\mathbf{J}_1]_{j,:} \left[ [\mathbf{J}_1, \mathbf{j}_{N_S-1+i}]^{-1} \right]_{1:N_S-1,:} \mathbf{r}_{N_S-1+i} \\ &\quad + Y_0 [\mathbf{j}_{N_S-1+i}]_j \left[ [\mathbf{J}_1, \mathbf{j}_{N_S-1+i}]^{-1} \right]_{N_S,:} \mathbf{r}_{N_S-1+i} \\ &= Y_0 [\mathbf{J}_1, \mathbf{j}_{N_S-1+i}]_{j,:} \left[ [\mathbf{J}_1, \mathbf{j}_{N_S-1+i}]^{-1} \right] \mathbf{r}_{N_S-1+i} \\ &= Y_0 [\mathbf{r}_{N_S-1+i}]_j = Y_0 [\mathbf{R}_2]_{j,i}, \end{aligned} \quad (45)$$

confirming that (42) and (43) are optimal solutions as they satisfy (41). Since  $\mathbf{B}_{22,12}$  is given by (43), we also know  $\mathbf{B}_{22,21}$ , which can be computed as  $\mathbf{B}_{22,21} = \mathbf{B}_{22,12}^T$ .

2) *Block  $\mathbf{B}_{22,11}$ :* We now need to find a symmetric matrix  $\mathbf{B}_{22,11}$  such that (40) is satisfied, i.e.,

$$\mathbf{J}_1 \mathbf{B}_{22,11} = Y_0 \mathbf{R}_1 - \mathbf{J}_2 \mathbf{B}_{22,21}, \quad (46)$$

where  $\mathbf{B}_{22,21}$  is given as  $\mathbf{B}_{22,21} = \mathbf{B}_{22,12}^T$ , with  $\mathbf{B}_{22,12}$  set according to (43). To solve the linear matrix equation in (46) where the unknown matrix is symmetric, we introduce the following result.

**Proposition 3.** Given two matrices  $\mathbf{A} \in \mathbb{R}^{M \times N}$  and  $\mathbf{C} \in$



**Algorithm 1** Optimization of a stem-connected MiLAC at the transmitter.

**Input:**  $\bar{\mathbf{V}}$ .

**Output:**  $\mathbf{B}$ .

$$\begin{aligned}
& \mathbf{R} = [\mathbf{R}_1, \mathbf{R}_2] = \Re \{ \bar{\mathbf{V}} \}^T, \mathbf{J} = [\mathbf{J}_1, \mathbf{J}_2] = \Im \{ \bar{\mathbf{V}} \}^T, \\
& \mathbf{r}_i = [\mathbf{R}]_{:,i}, \mathbf{j}_i = [\mathbf{J}]_{:,i}, \\
& \mathbf{J}_1 = [\mathbf{U}_{J,1}, \mathbf{u}_{J,2}] [\boldsymbol{\Sigma}_J, \mathbf{0}_{(N_S-1) \times 1}]^T \mathbf{V}_J^T, \\
& 1: [\mathbf{B}_{22,22}]_{i,i} = Y_0 [\mathbf{J}_1, \mathbf{j}_{N_S-1+i}]^{-1} \mathbf{r}_{N_S-1+i} \Big|_{N_S}, \\
& 2: [\mathbf{B}_{22,12}]_{j,i} = Y_0 [\mathbf{J}_1, \mathbf{j}_{N_S-1+i}]^{-1} \mathbf{r}_{N_S-1+i} \Big|_j, \\
& 3: \mathbf{B}_{22,21} = \mathbf{B}_{22,12}^T, \\
& 4: \mathbf{B}_{22,11} = \mathbf{V}_J \boldsymbol{\Sigma}_J^{-1} \mathbf{U}_{J,1}^T (Y_0 \mathbf{R}_1 - \mathbf{J}_2 \mathbf{B}_{22,21}), \\
& \mathbf{B}_{22} = [\mathbf{B}_{22,11}, \mathbf{B}_{22,12}]^T, [\mathbf{B}_{22,21}, \mathbf{B}_{22,22}]^T \Big]^T, \\
& 5: \mathbf{B}_{12} = -Y_0 \mathbf{J} - \mathbf{R} \mathbf{B}_{22}, \\
& 6: \mathbf{B}_{21} = \mathbf{B}_{12}^T, \\
& 7: \mathbf{B}_{11} = -\mathbf{R} \mathbf{B}_{21}, \\
& \mathbf{B} = [\mathbf{B}_{11}, \mathbf{B}_{12}]^T, [\mathbf{B}_{21}, \mathbf{B}_{22}]^T \Big]^T.
\end{aligned}$$

$\mathbb{R}^{M \times N}$ , consider the linear matrix equation

$$\mathbf{A}\mathbf{X} = \mathbf{C}, \quad (47)$$

where the unknown matrix  $\mathbf{X} \in \mathbb{R}^{N \times N}$  is constrained to be symmetric. The singular value decomposition (SVD) of  $\mathbf{A}$  is

$$\mathbf{A} = \mathbf{U} \begin{bmatrix} \boldsymbol{\Sigma} & \mathbf{0}_{R \times (N-R)} \\ \mathbf{0}_{(M-R) \times R} & \mathbf{0}_{(M-R) \times (N-R)} \end{bmatrix} \mathbf{V}^T, \quad (48)$$

where  $\mathbf{U} \in \mathbb{R}^{M \times M}$  contains the left singular vectors of  $\mathbf{A}$ ,  $\boldsymbol{\Sigma} \in \mathbb{R}^{R \times R}$  is a diagonal matrix containing the (positive) singular values of  $\mathbf{A}$ , with  $R$  being the rank of  $\mathbf{A}$ , and  $\mathbf{V} \in \mathbb{R}^{N \times N}$  contains the right singular vectors of  $\mathbf{A}$ . We partition  $\mathbf{U} = [\mathbf{U}_1, \mathbf{U}_2]$  with  $\mathbf{U}_1 \in \mathbb{R}^{M \times R}$  and  $\mathbf{U}_2 \in \mathbb{R}^{M \times (M-R)}$ , and  $\mathbf{V} = [\mathbf{V}_1, \mathbf{V}_2]$  with  $\mathbf{V}_1 \in \mathbb{R}^{N \times R}$  and  $\mathbf{V}_2 \in \mathbb{R}^{N \times (N-R)}$ . Thus, equation (47) has a symmetric solution if and only if  $\mathbf{A}\mathbf{C}^T = \mathbf{C}\mathbf{A}^T$  and  $\mathbf{U}_2^T \mathbf{C} = \mathbf{0}_{(M-R) \times N}$ . In this case, all solutions can be expressed as

$$\mathbf{X} = \mathbf{V}_1 \boldsymbol{\Sigma}^{-1} \mathbf{U}_1^T \mathbf{C} + \mathbf{V}_2 \mathbf{V}_2^T \mathbf{C}^T \mathbf{U}_1 \boldsymbol{\Sigma}^{-1} \mathbf{V}_1^T + \mathbf{V}_2 \mathbf{G} \mathbf{V}_2^T, \quad (49)$$

where  $\mathbf{G} \in \mathbb{R}^{(N-R) \times (N-R)}$  is any symmetric matrix.

*Proof.* This proposition follows from [26, Theorem 1].  $\square$

From Proposition 3, we can prove a useful corollary.

**Corollary 1.** Consider the setup of Proposition 3 with  $M = N+1$  and  $\mathbf{A}$  having full column rank, i.e., having rank  $R = N$ . Thus, equation (47) has a symmetric solution if and only if  $\mathbf{A}\mathbf{C}^T = \mathbf{C}\mathbf{A}^T$ . In this case, the only solution is given by

$$\mathbf{X} = \mathbf{V} \boldsymbol{\Sigma}^{-1} \mathbf{U}_1^T \mathbf{C}. \quad (50)$$

*Proof.* This corollary has two additional hypotheses beyond those in Proposition 3, i.e.,  $M = N+1$  and  $\mathbf{A}$  has full column rank, and states two different conclusions from Proposition 3. First, the necessary and sufficient condition for  $\mathbf{A}\mathbf{X} = \mathbf{C}$  to

have a symmetric solution is just  $\mathbf{A}\mathbf{C}^T = \mathbf{C}\mathbf{A}^T$  instead of  $\mathbf{A}\mathbf{C}^T = \mathbf{C}\mathbf{A}^T$  and  $\mathbf{u}_2^T \mathbf{C} = \mathbf{0}_{1 \times N}$ . Second, if  $\mathbf{A}\mathbf{X} = \mathbf{C}$  is solvable, it has only one symmetric solution instead of the infinitely many given by (49). Thus, to prove this corollary, it suffices to prove that i)  $\mathbf{A}\mathbf{C}^T = \mathbf{C}\mathbf{A}^T$  implies  $\mathbf{u}_2^T \mathbf{C} = \mathbf{0}_{1 \times N}$  if  $M = N+1$  and  $\mathbf{A}$  has full column rank, and ii) (49) boils down to (50) if  $M = N+1$  and  $\mathbf{A}$  has full column rank.

i) Since  $\mathbf{u}_2$  is the  $(N+1)$ th left singular vector of  $\mathbf{A}$ , which has rank  $N$ , we have  $\mathbf{u}_2^T \mathbf{A} = \mathbf{0}_{1 \times N}$ . Thus,  $\mathbf{A}\mathbf{C}^T = \mathbf{C}\mathbf{A}^T$  implies  $\mathbf{u}_2^T \mathbf{C}\mathbf{A}^T = \mathbf{0}_{1 \times (N+1)}$ . In turn,  $\mathbf{u}_2^T \mathbf{C}\mathbf{A}^T = \mathbf{0}_{1 \times (N+1)}$  implies  $\mathbf{u}_2^T \mathbf{C} = \mathbf{0}_{1 \times N}$  since  $\mathbf{A}$  has full column rank (recall that for any matrix  $\mathbf{A}$  having full column rank,  $\mathbf{k}\mathbf{A}^T = \mathbf{0}$  implies  $\mathbf{k} = \mathbf{0}$ ).

ii) It is easy to observe that (49) boils down to (50) if  $\mathbf{A}$  has full column rank, i.e.,  $\mathbf{V}_1 = \mathbf{V}$  and  $\mathbf{V}_2$  is empty.  $\square$

Corollary 1 can be applied to solve (46) since  $\mathbf{J}_1$  has dimensionality  $N_S \times (N_S - 1)$  and is full column rank with probability 1 given random channel realizations  $\mathbf{H}$ . Therefore, (46) has a symmetric solution  $\mathbf{B}_{22,11}$  if and only if

$$\mathbf{J}_1 (Y_0 \mathbf{R}_1 - \mathbf{J}_2 \mathbf{B}_{22,21})^T = (Y_0 \mathbf{R}_1 - \mathbf{J}_2 \mathbf{B}_{22,21}) \mathbf{J}_1^T, \quad (51)$$

which can be shown as follows

$$\mathbf{J}_1 (Y_0 \mathbf{R}_1 - \mathbf{J}_2 \mathbf{B}_{22,21})^T \quad (52)$$

$$= Y_0 \mathbf{J}_1 \mathbf{R}_1^T - \mathbf{J}_1 \mathbf{B}_{22,12} \mathbf{J}_2^T \quad (53)$$

$$\stackrel{a}{=} Y_0 \mathbf{R}_1 \mathbf{J}_1^T - Y_0 \mathbf{J}_2 \mathbf{R}_2^T + Y_0 \mathbf{R}_2 \mathbf{J}_2^T - \mathbf{J}_1 \mathbf{B}_{22,12} \mathbf{J}_2^T \quad (54)$$

$$\stackrel{b}{=} Y_0 \mathbf{R}_1 \mathbf{J}_1^T - Y_0 \mathbf{J}_2 \mathbf{R}_2^T + \mathbf{J}_2 \mathbf{B}_{22,22} \mathbf{J}_2^T \quad (55)$$

$$= Y_0 \mathbf{R}_1 \mathbf{J}_1^T - \mathbf{J}_2 (Y_0 \mathbf{R}_2^T - \mathbf{B}_{22,22} \mathbf{J}_2^T) \quad (56)$$

$$\stackrel{c}{=} Y_0 \mathbf{R}_1 \mathbf{J}_1^T - \mathbf{J}_2 \mathbf{B}_{22,21} \mathbf{J}_1^T \quad (57)$$

$$= (Y_0 \mathbf{R}_1 - \mathbf{J}_2 \mathbf{B}_{22,21}) \mathbf{J}_1^T, \quad (58)$$

where  $\stackrel{a}{=}$  holds since  $\mathbf{R}_1 \mathbf{J}_1^T + \mathbf{R}_2 \mathbf{J}_2^T = \mathbf{J}_1 \mathbf{R}_1^T + \mathbf{J}_2 \mathbf{R}_2^T$ , which follows from  $\mathbf{R}\mathbf{J}^T = \mathbf{J}\mathbf{R}^T$ , verified since  $\Re\{\bar{\mathbf{V}}\}^T \Im\{\bar{\mathbf{V}}\} = \Im\{\bar{\mathbf{V}}\}^T \Re\{\bar{\mathbf{V}}\}$  for any unitary matrix  $\mathbf{V} = [\bar{\mathbf{V}}, \tilde{\mathbf{V}}]$ ,  $\stackrel{b}{=}$  exploits  $\mathbf{J}_2 \mathbf{B}_{22,22} \mathbf{J}_2^T = Y_0 \mathbf{R}_2 \mathbf{J}_2^T - \mathbf{J}_1 \mathbf{B}_{22,12} \mathbf{J}_2^T$  which follows from (41),  $\stackrel{c}{=}$  exploits  $(\mathbf{J}_1 \mathbf{B}_{22,12})^T = (Y_0 \mathbf{R}_2 - \mathbf{J}_2 \mathbf{B}_{22,22})^T$  following from (41), and the other equalities are straightforward. Since we have verified (51), Corollary 1 states that (46) has a unique symmetric solution as a function of the SVD of  $\mathbf{J}_1$  and the matrix  $Y_0 \mathbf{R}_1 - \mathbf{J}_2 \mathbf{B}_{22,21}$ . Let the SVD of  $\mathbf{J}_1$  be

$$\mathbf{J}_1 = \mathbf{U}_J \begin{bmatrix} \boldsymbol{\Sigma}_J \\ \mathbf{0}_{1 \times (N_S-1)} \end{bmatrix} \mathbf{V}_J^T, \quad (59)$$

where the matrix of left singular vectors  $\mathbf{U}_J \in \mathbb{R}^{N_S \times N_S}$  is partitioned into  $\mathbf{U}_J = [\mathbf{U}_{J,1}, \mathbf{U}_{J,2}]$  with  $\mathbf{U}_{J,1} \in \mathbb{R}^{N_S \times (N_S-1)}$  and  $\mathbf{u}_{J,2} \in \mathbb{R}^{N_S \times 1}$ ,  $\boldsymbol{\Sigma}_J \in \mathbb{R}^{(N_S-1) \times (N_S-1)}$  is a diagonal matrix containing the (positive) singular values, and  $\mathbf{V}_J \in \mathbb{R}^{(N_S-1) \times (N_S-1)}$  is the matrix of right singular vectors. Thus,  $\mathbf{B}_{22,11}$  is given by

$$\mathbf{B}_{22,11} = \mathbf{V}_J \boldsymbol{\Sigma}_J^{-1} \mathbf{U}_{J,1}^T (Y_0 \mathbf{R}_1 - \mathbf{J}_2 \mathbf{B}_{22,21}), \quad (60)$$

according to Corollary 1.

We can now assemble the block  $\mathbf{B}_{22}$  following (38) since we have derived the blocks  $\mathbf{B}_{22,12}$ ,  $\mathbf{B}_{22,21}$ , and  $\mathbf{B}_{22,22}$  in Section V-B1, and the block  $\mathbf{B}_{22,11}$  in Section V-B2.

### C. Blocks $\mathbf{B}_{11}$ , $\mathbf{B}_{12}$ , and $\mathbf{B}_{21}$

In Section V-B, we have derived in closed form the optimal value of the admittance matrix block  $\mathbf{B}_{22}$ . With  $\mathbf{B}_{22}$  known, the remaining blocks of the admittance matrix  $\mathbf{B}_{12}$ ,  $\mathbf{B}_{21}$ , and  $\mathbf{B}_{11}$ , can be readily obtained as follows. First,  $\mathbf{B}_{12}$  can be found as a function of  $\mathbf{B}_{22}$  by using (37), i.e.,

$$\mathbf{B}_{12} = -Y_0 \mathbf{J} - \mathbf{R} \mathbf{B}_{22}. \quad (61)$$

Second, recalling that  $\mathbf{B}$  is symmetric, we have

$$\mathbf{B}_{21} = \mathbf{B}_{12}^T, \quad (62)$$

with  $\mathbf{B}_{12}$  set as in (61). Third, the remaining block  $\mathbf{B}_{11}$  can be found through (36) as

$$\mathbf{B}_{11} = -\mathbf{R} \mathbf{B}_{21}, \quad (63)$$

with  $\mathbf{B}_{21}$  given by (62).

We can now assemble  $\mathbf{B}$  following (28) since we have derived all its four blocks. In Alg. 1, we summarize the algorithm that allows us to find in closed form a capacity-achieving solution to the admittance matrix  $\mathbf{B}$  of a stem-connected MiLAC at the transmitter.

### D. Checking Solution Optimality

Note that the solution in Alg. 1 is guaranteed by design to fulfill all the constraints of the feasibility check problem (31)-(37) except for two constraints that have not been used throughout our solution, namely *i)*  $\mathbf{B}_{11} = \mathbf{B}_{11}^T$  and *ii)*  $\mathbf{J} \mathbf{B}_{21} = -Y_0 \mathbf{I}_{N_S}$ . For completeness, we show that these two constraints are satisfied in the following. First, considering the block  $\mathbf{B}_{11}$  set as in (63), we have

$$\mathbf{B}_{11}^T = -\mathbf{B}_{21}^T \mathbf{R}^T \stackrel{a}{=} Y_0 \mathbf{J} \mathbf{R}^T + \mathbf{R} \mathbf{B}_{22} \mathbf{R}^T \quad (64)$$

$$\stackrel{b}{=} Y_0 \mathbf{R} \mathbf{J}^T + \mathbf{R} \mathbf{B}_{22} \mathbf{R}^T \quad (65)$$

$$= \mathbf{R} (Y_0 \mathbf{J}^T + \mathbf{B}_{22} \mathbf{R}^T) \quad (66)$$

$$\stackrel{c}{=} -\mathbf{R} \mathbf{B}_{21} = \mathbf{B}_{11}, \quad (67)$$

where  $\stackrel{a}{=}$  follows from (61) and (62),  $\stackrel{b}{=}$  follows from  $\mathbf{R} \mathbf{J}^T = \mathbf{J} \mathbf{R}^T$ , verified since  $\Re\{\bar{\mathbf{V}}\}^T \Im\{\bar{\mathbf{V}}\} = \Im\{\bar{\mathbf{V}}\}^T \Re\{\bar{\mathbf{V}}\}$  for any unitary matrix  $\mathbf{V} = [\bar{\mathbf{V}}, \hat{\mathbf{V}}]$ , and  $\stackrel{c}{=}$  follows from  $\mathbf{B}_{22} = \mathbf{B}_{22}^T$ , (61), and (62), confirming that  $\mathbf{B}_{11} = \mathbf{B}_{11}^T$ . Second, considering the block  $\mathbf{B}_{21}$  set as in (62), we have

$$\mathbf{J} \mathbf{B}_{21} = \mathbf{J} \mathbf{B}_{12}^T \stackrel{a}{=} -\mathbf{J} (Y_0 \mathbf{J} + \mathbf{R} \mathbf{B}_{22})^T \quad (68)$$

$$\stackrel{b}{=} -Y_0 \mathbf{J} \mathbf{J}^T - \mathbf{J} \mathbf{B}_{22} \mathbf{R}^T \quad (69)$$

$$\stackrel{c}{=} -Y_0 \mathbf{J} \mathbf{J}^T - Y_0 \mathbf{R} \mathbf{R}^T \stackrel{d}{=} -Y_0 \mathbf{I}_{N_S}, \quad (70)$$

where  $\stackrel{a}{=}$  follows from (61),  $\stackrel{b}{=}$  follows from  $\mathbf{B}_{22} = \mathbf{B}_{22}^T$ ,  $\stackrel{c}{=}$  follows from (35), and  $\stackrel{d}{=}$  follows from  $\mathbf{J} \mathbf{J}^T + \mathbf{R} \mathbf{R}^T = \mathbf{I}_{N_S}$ , verified since  $\Im\{\bar{\mathbf{V}}\}^T \Im\{\bar{\mathbf{V}}\} + \Re\{\bar{\mathbf{V}}\}^T \Re\{\bar{\mathbf{V}}\} = \mathbf{I}$  for any unitary matrix  $\mathbf{V} = [\bar{\mathbf{V}}, \hat{\mathbf{V}}]$ , confirming that  $\mathbf{J} \mathbf{B}_{21} = -Y_0 \mathbf{I}_{N_S}$ .

## VI. OPTIMIZATION OF CAPACITY-ACHIEVING RECEIVER-SIDE MiLAC ARCHITECTURES

In Section V, we have proven Proposition 1 by deriving a capacity-achieving solution to optimize stem-connected MiLACs at the transmitter. In this section, we prove Proposition 2

by extending the discussion of Section V to stem-connected MiLACs at the receiver. Although the optimization of receiver-side MiLACs is analogous to that of transmitter-side MiLACs, it requires a different partition of the MiLAC admittance matrix and hence deserves separate consideration. To simplify the notation, only in this section, we denote the scattering, admittance, and susceptance matrices of the considered MiLAC at the receiver as  $\Theta$ ,  $\mathbf{Y}$ , and  $\mathbf{B}$  instead of  $\Theta_G$ ,  $\mathbf{Y}_G$ , and  $\mathbf{B}_G$ .

### A. Reformulation of the Capacity-Achieving Condition

Recalling that  $\Theta$  can be expressed as a function of the admittance matrix  $\mathbf{Y} = j\mathbf{B}$  as in (3), the capacity-achieving condition in (17) can be rewritten as

$$(Y_0 \mathbf{I} - j\mathbf{B}) \begin{bmatrix} \mathbf{0}_{N_T \times N_S} \\ \mathbf{I}_{N_S} \end{bmatrix} = (Y_0 \mathbf{I} + j\mathbf{B}) \begin{bmatrix} \bar{\mathbf{U}}^* \\ \mathbf{0}_{N_S} \end{bmatrix}, \quad (71)$$

as a function of  $\mathbf{B}$ , which can be simplified as

$$j\mathbf{B} \begin{bmatrix} \bar{\mathbf{U}}^* \\ \mathbf{I}_{N_S} \end{bmatrix} = Y_0 \begin{bmatrix} -\bar{\mathbf{U}}^* \\ \mathbf{I}_{N_S} \end{bmatrix}, \quad (72)$$

or, equivalently,

$$j \begin{bmatrix} \bar{\mathbf{U}}^H & \mathbf{I}_{N_S} \end{bmatrix} \mathbf{B} = Y_0 \begin{bmatrix} -\bar{\mathbf{U}}^H & \mathbf{I}_{N_S} \end{bmatrix}, \quad (73)$$

given the symmetry of  $\mathbf{B}$ . Since (73) is a linear matrix equation with real unknowns and complex coefficients, we rewrite it in real coefficients as

$$\begin{bmatrix} \Re\{j \begin{bmatrix} \bar{\mathbf{U}}^H & \mathbf{I}_{N_S} \end{bmatrix} \mathbf{B}\} \\ \Im\{j \begin{bmatrix} \bar{\mathbf{U}}^H & \mathbf{I}_{N_S} \end{bmatrix} \mathbf{B}\} \end{bmatrix} = \begin{bmatrix} \Re\{Y_0 \begin{bmatrix} -\bar{\mathbf{U}}^H & \mathbf{I}_{N_S} \end{bmatrix}\} \\ \Im\{Y_0 \begin{bmatrix} -\bar{\mathbf{U}}^H & \mathbf{I}_{N_S} \end{bmatrix}\} \end{bmatrix}, \quad (74)$$

which simplifies to

$$\begin{bmatrix} \Im\{\bar{\mathbf{U}}\}^T & \mathbf{0}_{N_S} \\ \Re\{\bar{\mathbf{U}}\}^T & \mathbf{I}_{N_S} \end{bmatrix} \mathbf{B} = Y_0 \begin{bmatrix} -\Re\{\bar{\mathbf{U}}\}^T & \mathbf{I}_{N_S} \\ \Im\{\bar{\mathbf{U}}\}^T & \mathbf{0}_{N_S} \end{bmatrix}. \quad (75)$$

Similar to what done at the transmitter-side in Section V, we consider the partition of  $\mathbf{B}$  in (28), where  $\mathbf{B}_{11} \in \mathbb{R}^{N_R \times N_R}$ ,  $\mathbf{B}_{12} \in \mathbb{R}^{N_R \times N_S}$ ,  $\mathbf{B}_{21} \in \mathbb{R}^{N_S \times N_R}$ , and  $\mathbf{B}_{22} \in \mathbb{R}^{N_S \times N_S}$ , and introduce  $\mathbf{R} \in \mathbb{R}^{N_S \times N_R}$  and  $\mathbf{J} \in \mathbb{R}^{N_S \times N_R}$  as  $\mathbf{R} = \Re\{\bar{\mathbf{U}}\}^T$  and  $\mathbf{J} = \Im\{\bar{\mathbf{U}}\}^T$ , such that (75) becomes

$$\begin{bmatrix} \mathbf{J} & \mathbf{0}_{N_S} \\ \mathbf{R} & \mathbf{I}_{N_S} \end{bmatrix} \begin{bmatrix} \mathbf{B}_{11} & \mathbf{B}_{12} \\ \mathbf{B}_{21} & \mathbf{B}_{22} \end{bmatrix} = Y_0 \begin{bmatrix} -\mathbf{R} & \mathbf{I}_{N_S} \\ \mathbf{J} & \mathbf{0}_{N_S} \end{bmatrix}. \quad (76)$$

To formalize the constraints on the blocks  $\mathbf{B}_{11}$ ,  $\mathbf{B}_{12}$ ,  $\mathbf{B}_{21}$ , and  $\mathbf{B}_{22}$ , we assume with no loss of generality that the considered stem-connected MiLAC has the  $N_S - 1$  input ports  $V_1, \dots, V_{N_S-1}$  connected to all the others, as Fig. 4(a). With this assumption, we have  $\mathbf{B} \in \mathcal{B}_G$ , where  $\mathcal{B}_G$  is given by (19). Consequently, the only constraints on  $\mathbf{B}_{12}$ ,  $\mathbf{B}_{21}$ , and  $\mathbf{B}_{22}$  are  $\mathbf{B}_{21} = \mathbf{B}_{12}^T$  and  $\mathbf{B}_{22} = \mathbf{B}_{22}^T$  (due to the symmetry of  $\mathbf{B}$ , and since the  $N_S$  output ports of the MiLAC are connected to all the others as required by Proposition 2), while  $\mathbf{B}_{11}$  satisfies  $\mathbf{B}_{11} = \mathbf{B}_{11}^T$  and  $\mathbf{B}_{11} \in \mathcal{B}_{11}$ , where

$$\mathcal{B}_{11} = \left\{ \mathbf{B} \in \mathbb{R}^{N_R \times N_R} \mid [\mathbf{B}]_{n,m} = 0, \forall n \neq m, \right. \\ \left. n > N_S - 1, m > N_S - 1 \right\}. \quad (77)$$

$$\mathbf{B} = \left[ [\mathbf{B}_{11}, \mathbf{B}_{12}]^T, [\mathbf{B}_{21}, \mathbf{B}_{22}]^T \right]^T.$$

as a function of the SVD of  $\mathbf{J}_1$  in (59).

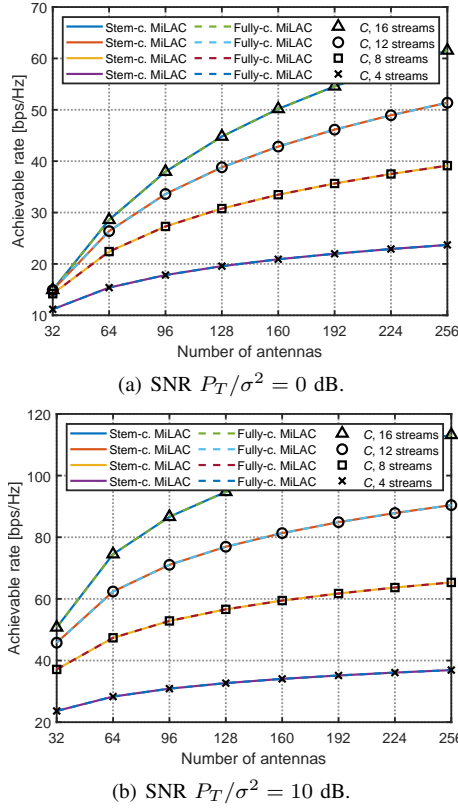


Fig. 7. Achievable rate versus the number of antennas  $N_T = N_R$ , for different numbers of streams  $N_S$ , and values of SNR  $P_T/\sigma^2$ . The achievable rate of stem- and fully-connected MiLAC, and the capacity in (9) are compared.

Given the blocks  $\mathbf{B}_{11,12}$ ,  $\mathbf{B}_{11,21}$ , and  $\mathbf{B}_{11,22}$  derived in Section VI-B1, and the block  $\mathbf{B}_{11,11}$  derived in Section VI-B2, we can now assemble  $\mathbf{B}_{11}$  according to (85).

### C. Blocks $\mathbf{B}_{12}$ , $\mathbf{B}_{21}$ , and $\mathbf{B}_{22}$

With the block  $\mathbf{B}_{11}$  derived in Section VI-B, we can compute  $\mathbf{B}_{21}$  by using (83), i.e.,

$$\mathbf{B}_{21} = \mathbf{Y}_0 \mathbf{J} - \mathbf{R} \mathbf{B}_{11}, \quad (94)$$

and, recalling that  $\mathbf{B}$  is symmetric, we also have

$$\mathbf{B}_{12} = \mathbf{B}_{21}^T. \quad (95)$$

Then, the remaining block  $\mathbf{B}_{22}$  can be found through (84) as

$$\mathbf{B}_{22} = -\mathbf{R} \mathbf{B}_{12}, \quad (96)$$

with  $\mathbf{B}_{12}$  given by (95).

Finally,  $\mathbf{B}$  is readily given by (28) since we have derived all its four blocks. In Alg. 2, we summarize the steps leading to a capacity-achieving solution for the admittance matrix  $\mathbf{B}$  of a stem-connected MiLAC at the receiver.

### D. Checking Solution Optimality

The solution in Alg. 2 is guaranteed by design to fulfill all the constraints of the feasibility check problem (78)-(84) except for two constraints that have not been used throughout our solution, namely i)  $\mathbf{B}_{22} = \mathbf{B}_{22}^T$  and ii)  $\mathbf{J} \mathbf{B}_{12} = \mathbf{Y}_0 \mathbf{I}_{N_S}$ .

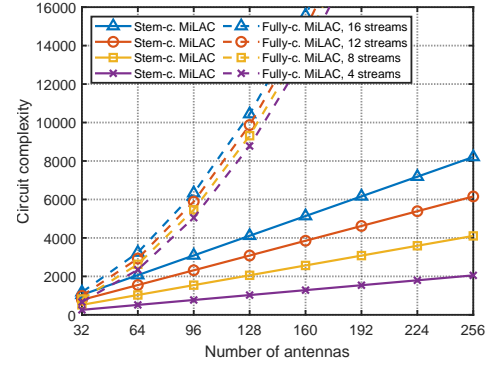


Fig. 8. Circuit complexity of stem- and fully-connected MiLAC versus the number of antennas ( $N_T$  or  $N_R$ ), for different numbers of streams  $N_S$ .

Interestingly, also these two constraints are satisfied, as it can be shown by proofs similar to those in Section V-D, which are omitted for conciseness.

## VII. NUMERICAL RESULTS

We have proposed a novel family of MiLAC architectures, named stem-connected MiLAC, and provided a closed-form capacity-achieving solution to optimize it at the transmitter and receiver sides in Sections V and VI, respectively. In this section, we validate the optimality of the proposed solution through Monte Carlo simulations and compare stem- and fully-connected MiLACs in terms of performance and circuit complexity.

In Fig. 7, we report the achievable rate obtained with stem-connected and fully-connected MiLACs averaged over sufficient realizations of independent and identically distributed (i.i.d.) Rayleigh fading channels, i.e.,  $\text{vec}(\mathbf{H}) \sim \mathcal{CN}(\mathbf{0}_{N_R N_T \times 1}, \mathbf{I}_{N_R N_T \times 1})$ . We consider different scenarios where  $N_R = N_T$ , the number of streams is  $N_S \in \{4, 8, 12, 16\}$  and the signal-to-noise ratio (SNR) is  $P_T/\sigma^2 \in \{0, 10\}$  dB. For each scenario, we compare: the achievable rate with stem-connected MiLACs at the transmitter and receiver sides optimized with the solutions proposed in Sections V and VI, the achievable rate with fully-connected MiLACs optimized as proposed in [20], and the capacity in (9). In agreement with our theoretical analysis, we observe that stem-connected MiLACs achieve the same rate as fully-connected MiLACs, corresponding to the capacity derived in (9). Thus, while maintaining the maximum performance, stem-connected MiLACs can provide enormous gains in terms of circuit complexity.

In Fig. 8, we report the circuit complexity, i.e., the number of admittance components, of a stem-connected MiLACs  $N_C^{\text{Stem}}$  with center size  $Q = 2N_S - 1$  given by (22), and of a fully-connected MiLAC  $N_C^{\text{Fully}}$  given by (15). The circuit complexity is reported versus the number of antennas ( $N_T$  for a MiLAC at the transmitter or  $N_R$  for a MiLAC at the receiver), for different values of the number of streams  $N_S$ . We make the following three observations. *First*, the circuit complexity of both fully- and stem-connected MiLACs increases with the number of streams and the number of antennas. *Second*, with a fixed number of streams  $N_S$ , the circuit

complexity of a fully-connected MiLAC scales quadratically with the number of antennas, i.e.,  $N_C^{\text{Fully}} = \mathcal{O}((N_S + N_T)^2)$  or  $N_C^{\text{Fully}} = \mathcal{O}((N_S + N_R)^2)$  for a MiLAC at the transmitter or at the receiver, respectively. *Third*, with a fixed  $N_S$ , the circuit complexity of a stem-connected MiLAC scales linearly with the number of antennas, i.e.,  $N_C^{\text{Stem}} = \mathcal{O}(N_S N_T)$  or  $N_C^{\text{Stem}} = \mathcal{O}(N_S N_R)$  for a MiLAC at the transmitter or at the receiver, respectively. Thus, a stem-connected MiLAC can achieve the same capacity as a fully-connected MiLAC, simplifying significantly the hardware when the number of antennas grows large.

### VIII. CONCLUSION

The concept of MiLAC has recently emerged to enable gigantic MIMO by performing signal processing and beamforming entirely in the analog domain via multiport microwave networks. However, previous work has explored MiLAC architectures, denoted as fully-connected MiLACs, which include tunable impedance components interconnecting all MiLAC ports to each other. Hence, their circuit complexity, measured in terms of the number of required impedance components, scales quadratically with the number of antennas, limiting their practicality. In this paper, we address this scalability issue by proposing a graph theoretical model of MiLAC that allows us to explore lower-complexity MiLAC architectures. We model a MiLAC as a graph, whose vertices represent the MiLAC ports and edges represent the presence of impedance components interconnecting the ports. Through this graph theoretical model, we characterize a family of MiLAC architectures, denoted as stem-connected MiLACs, which maintains the capacity-achieving property of fully-connected MiLACs, while significantly reducing the circuit complexity. To show that stem-connected MiLACs are capacity-achieving, we optimize them through a closed-form solution that is proven to globally maximize the achievable rate for any channel realization, i.e., to reach the capacity. Simulation results support our theoretical analysis and demonstrate that stem-connected MiLACs can achieve the same capacity as fully-connected MiLACs, which corresponds to the capacity achievable with a fully-digital MIMO system with the same number of streams. At the same time, stem-connected MiLACs are characterized by a circuit complexity scaling linearly with the number of antennas, rather than quadratically, making them a practical and scalable solution to enable high-performance gigantic MIMO systems.

In this study, we have proposed low-complexity MiLAC architectures that are proven to achieve capacity in point-to-point MIMO systems, and we have developed an algorithm to globally optimize them. A promising direction for future research is to investigate whether the proposed MiLAC architectures remain optimal in multi-user communication systems, and to develop optimization strategies for such scenarios.

### REFERENCES

- [1] F. Boccardi, R. W. Heath, A. Lozano, T. L. Marzetta, and P. Popovski, "Five disruptive technology directions for 5G," *IEEE Commun. Mag.*, vol. 52, no. 2, pp. 74–80, 2014.
- [2] E. G. Larsson, O. Edfors, F. Tufvesson, and T. L. Marzetta, "Massive MIMO for next generation wireless systems," *IEEE Commun. Mag.*, vol. 52, no. 2, pp. 186–195, 2014.
- [3] Qualcomm. (2022) Vision, market drivers, and research directions on the path to 6G. [Online]. Available: <https://www.qualcomm.com/research/6g>
- [4] E. Björnson, F. Kara, N. Kolomvakis, A. Kosasih, P. Ramezani, and M. B. Salman, "Enabling 6G performance in the upper mid-band by transitioning from massive to gigantic MIMO," *arXiv preprint arXiv:2407.05630*, 2024.
- [5] O. E. Ayach, S. Rajagopal, S. Abu-Surra, Z. Pi, and R. W. Heath, "Spatially sparse precoding in millimeter wave MIMO systems," *IEEE Trans. Wireless Commun.*, vol. 13, no. 3, pp. 1499–1513, 2014.
- [6] F. Sohrabi and W. Yu, "Hybrid digital and analog beamforming design for large-scale antenna arrays," *IEEE J. Sel. Top. Signal Process.*, vol. 10, no. 3, pp. 501–513, 2016.
- [7] R. L. Haupt and M. Lanagan, "Reconfigurable antennas," *IEEE Antennas Propag. Mag.*, vol. 55, no. 1, pp. 49–61, 2013.
- [8] M. R. Castellanos, S. Yang, C.-B. Chae, and R. W. Heath Jr, "Embracing reconfigurable antennas in the tri-hybrid MIMO architecture for 6G," *arXiv preprint arXiv:2501.16610*, 2025.
- [9] Q. Wu, S. Zhang, B. Zheng, C. You, and R. Zhang, "Intelligent reflecting surface-aided wireless communications: A tutorial," *IEEE Trans. Commun.*, vol. 69, no. 5, pp. 3313–3351, 2021.
- [10] Y. Huang, L. Zhu, and R. Zhang, "Integrating intelligent reflecting surface into base station: Architecture, channel model, and passive reflection design," *IEEE Trans. Commun.*, vol. 71, no. 8, pp. 5005–5020, 2023.
- [11] S. Shen, B. Clerckx, and R. Murch, "Modeling and architecture design of reconfigurable intelligent surfaces using scattering parameter network analysis," *IEEE Trans. Wireless Commun.*, vol. 21, no. 2, pp. 1229–1243, 2022.
- [12] H. Li, S. Shen, M. Nerini, and B. Clerckx, "Reconfigurable intelligent surfaces 2.0: Beyond diagonal phase shift matrices," *IEEE Commun. Mag.*, vol. 62, no. 3, pp. 102–108, 2024.
- [13] A. Mishra, Y. Mao, C. D'Andrea, S. Buzzi, and B. Clerckx, "Transmitter side beyond-diagonal reconfigurable intelligent surface for massive MIMO networks," *IEEE Wireless Commun. Lett.*, vol. 13, no. 2, pp. 352–356, 2024.
- [14] J. An, C. Xu, D. W. K. Ng, G. C. Alexandropoulos, C. Huang, C. Yuen, and L. Hanzo, "Stacked intelligent metasurfaces for efficient holographic MIMO communications in 6G," *IEEE J. Sel. Areas Commun.*, vol. 41, no. 8, pp. 2380–2396, 2023.
- [15] J. An, M. D. Renzo, M. Debbah, H. Vincent Poor, and C. Yuen, "Stacked intelligent metasurfaces for multiuser downlink beamforming in the wave domain," *IEEE Trans. Wireless Commun.*, 2025.
- [16] N. Shlezinger, G. C. Alexandropoulos, M. F. Imani, Y. C. Eldar, and D. R. Smith, "Dynamic metasurface antennas for 6G extreme massive MIMO communications," *IEEE Wireless Commun.*, vol. 28, no. 2, pp. 106–113, 2021.
- [17] H. Prod'homme and P. del Hougne, "Beyond-diagonal dynamic metasurface antenna," *arXiv preprint arXiv:2504.13523*, 2025.
- [18] M. Nerini and B. Clerckx, "Analog computing for signal processing and communications – Part I: Computing with microwave networks," *arXiv preprint arXiv:2504.06790*, 2025.
- [19] M. Nerini and B. Clerckx, "Analog computing for signal processing and communications – Part II: Toward gigantic MIMO beamforming," *arXiv preprint arXiv:2504.07477*, 2025.
- [20] M. Nerini and B. Clerckx, "Capacity of MIMO systems aided by microwave linear analog computers (MiLACs)," *arXiv preprint arXiv:2506.05983*, 2025.
- [21] D. M. Pozar, *Microwave engineering*. John Wiley & Sons, 2011.
- [22] M. Nerini, S. Shen, H. Li, and B. Clerckx, "Beyond diagonal reconfigurable intelligent surfaces utilizing graph theory: Modeling, architecture design, and optimization," *IEEE Trans. Wireless Commun.*, vol. 23, no. 8, pp. 9972–9985, 2024.
- [23] J. A. Bondy and U. S. R. Murty, *Graph theory with applications*. Macmillan London, 1976, vol. 290.
- [24] X. Zhou, T. Fang, and Y. Mao, "A novel Q-stem connected architecture for beyond-diagonal reconfigurable intelligent surfaces," *arXiv preprint arXiv:2411.18480*, 2024.
- [25] Z. Wu and B. Clerckx, "Beyond diagonal RIS in multiuser MIMO: Graph theoretic modeling and optimal architectures with low complexity," *arXiv preprint arXiv:2502.16509*, 2025.
- [26] D. Hua, "On the symmetric solutions of linear matrix equations," *Linear Algebra and its Applications*, vol. 131, pp. 1–7, 1990.